Applied Physics Letters

Demonstration of single-phase wurtzite BAlN with over 20% boron content by metalorganic chemical vapor deposition

Cite as: Appl. Phys. Lett. **117**, 082102 (2020); https://doi.org/10.1063/5.0019881
Submitted: 26 June 2020 . Accepted: 10 August 2020 . Published Online: 27 August 2020

Tinh Binh Tran, Che-Hao Liao, Feras AlQatari, and Xiaohang Li

Applied Physics Letters ARTICLE scitation.org/journal/apl

Demonstration of single-phase wurtzite BAlN with over 20% boron content by metalorganic chemical vapor deposition

Cite as: Appl. Phys. Lett. **117**, 082102 (2020); doi: 10.1063/5.0019881
Submitted: 26 June 2020 · Accepted: 10 August 2020 ·
Published Online: 27 August 2020

Tinh Binh Tran,[a] Che-Hao Liao, Feras AlQatari, and Xiaohang Li[a]

AFFILIATIONS

King Abdullah University of Science and Technology (KAUST), Advanced Semiconductor Laboratory, Thuwal 23955, Saudi Arabia

Note: This paper is part of the Special Topic on Ultrawide Bandgap Semiconductors.
[a]**Authors to whom correspondence should be addressed:** tinh.tran@kaust.edu.sa and xiaohang.li@kaust.edu.sa

ABSTRACT

Wurtzite BAlN alloys are emerging ultrawide bandgap III-nitride semiconductors promising for optical and electronic devices. Yet the boron compositions of the grown alloys have been limited. In this Letter, we report on the demonstration of a thick single-phase wurtzite BAlN film with a boron composition over 20%. The growth was conducted at 1010 °C and 150 Torr with continuous flows of group-III precursors and ammonia with a growth rate of 2.2 μm/h by metalorganic chemical vapor deposition. The boron composition was studied by x-ray diffraction (XRD), secondary neutral mass spectrometry (SNMS), and Rutherford backscattering spectrometry (RBS). The XRD 2θ scan exhibited the clear wurtzite BAlN peak 1.82° larger than the AlN peak, indicating the boron composition of 30.9% based on the lattice constants of wurtzite AlN and BN. The SNMS and RBS experiments, independent of strain and defects, revealed that the boron content was 22%. The microstructures of the wurtzite BAlN film were further studied by transmission electron microscopy, showing an initial 5 nm thick layer free of crystal twinning followed by widespread crystal twinning with lattice rotations of 60° clockwise and anti-clockwise. The optical transmission experiment manifested that the bandgap of the smaller-lattice BAlN film was 5.1 eV, smaller than that of larger-lattice AlN. This trend was the opposite of the conventional InGaAlN but consistent with theoretical predictions. This study would greatly facilitate the research of material, physics, and devices incorporating the wurtzite BAlN alloys.

Wurtzite BAlN alloys are emerging ultrawide bandgap III-nitride semiconductors. Due to their unique properties such as lattice, optical, and polarization constants, they are promising for potential applications in UV devices, distributed Bragg reflectors (DBRs), power electronic devices, radiation tolerant electronics, and other optoelectronic components.[1–9] However, at present many epitaxial challenges need to be addressed to achieve high quality and to increase the boron content while maintaining the wurtzite phase, such as phase separation, limited thin film thickness, and limited adatom diffusion length.[10–15] The boron content of the wurtzite BAlN alloys has been limited to less than 15% with a relatively small thickness of 100 nm, which greatly limits the device applications of the BAlN alloys.[1]

In this Letter, we report on the growth of a 360 nm single-phase wurtzite BAlN thin film with the boron composition of 22% on an AlN/sapphire template by metalorganic chemical vapor deposition (MOCVD). The epitaxial growth was carried out in a Taiyo Nippon Sanso SR-4000HT horizontal MOCVD system on a c-plane sapphire substrate. Trimethylaluminum (TMA), triethylboron (TEB), and ammonia (NH_3) were used as precursors with hydrogen (H_2) as the carrier gas. First, a 3.5 μm thick AlN template was grown on sapphire. The (002) and (102) FWHMs of the x-ray diffraction (XRD) rocking curves of the template were 200 and 355 arc sec, respectively. The RMS surface roughness of the AlN template was 0.7 nm from the 5×5 μm^2 atomic force microscopy (AFM) scan [Fig. 1(a)]. The BAlN film was subsequently grown at 1010 °C at 150 Torr with continuous flows of TMA, TEB, and NH_3. The V/III ratio was 1896 with the TEB/(TEB+TMA) molar flow ratio of 0.73. The estimated growth rate of the BAlN film was 2.2 μm/h with a thickness of 360 nm. This growth condition might seem to significantly deviate from what we reported before for wurtzite BAlN grown by the AIXTRON close-coupled showerhead MOCVD system.[1] However, it is due to the use of a different Taiyo Nippon Sanso horizontal MOCVD system and, thus, different optimized growth conditions including the V/III ratio. Figure 1(b) shows the surface morphology of the BAlN film with the increased RMS surface roughness of 2.7 nm from the 5×5 μm^2 AFM image.

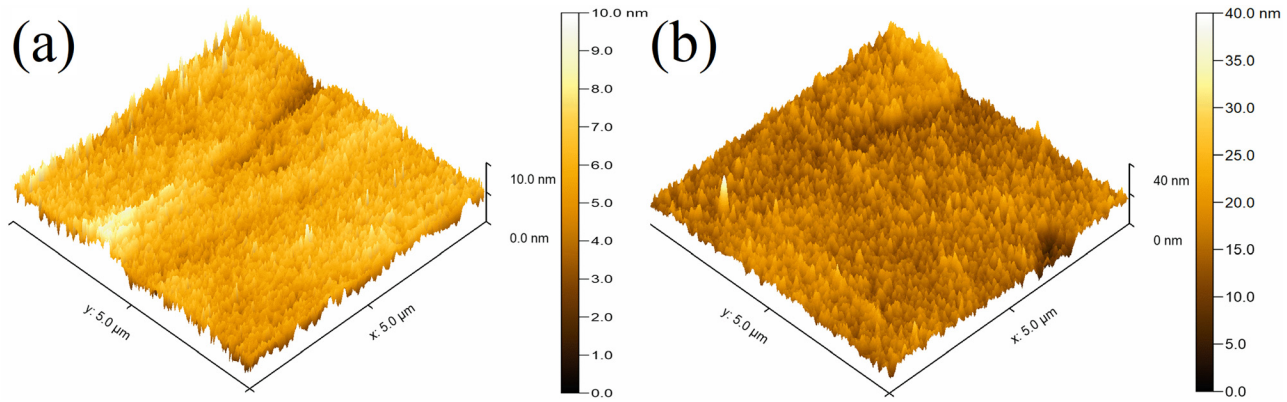

FIG. 1. AFM images of (a) the AlN/sapphire template and (b) the BAlN film grown on the template.

To study the boron composition and the crystallinity, the sample was analyzed by the (002) 2θ–ω XRD scan using the CuK_{a1} line (1.54 Å) of the Bruker D8 Ultra XRD system shown in Fig. 2. The peaks of AlN and sapphire are strong at 36.02° and 41.61°, while a weaker but distinct BAlN peak is observed at 37.90°, demonstrating the wurtzite phase. Thus, the 2θ angular separation of the AlN and BAlN peaks is 1.82°, which is much larger than the 0.58° angular separation for wurtzite $B_{0.144}Al_{0.856}N$ reported by Li *et al.*[1] This indicates a much larger solubility limit than previously thought.[10] The corresponding lattice constants of the AlN template and the BAlN film are 4.98 and 4.74 Å according to the Bragg condition. By applying Vegard's law using the reported lattice constants of wurtzite BN,[16] the boron content of the BAlN film was estimated to be 30.9%. No additional peaks were observed in Fig. 2 with the 2θ angle ranging from 30° to 41°, indicating the wurtzite phase without considerable compositional inhomogeneity or phase separation in the BAlN film.

As material defects and strain and alloy bowing could affect the film thickness and the material composition estimated by XRD using Vegard's law,[1] a Dynamic system from HIDEN Analytical Ltd was employed using the secondary ion mass spectroscopy (SIMS) and the secondary neutral mass spectroscopy (SNMS) modes.[17–19] Figure 3(a) shows that the boron and aluminum signals are stable from the surface to 360 nm, indicating homogeneous boron and aluminum compositions in the BAlN film, and the boron signal then drops drastically beyond 360 nm, suggesting the AlN template. Thus, the BAlN film thickness is 360 nm. The SNMS result in Fig. 3(b) manifests that the boron and aluminum concentrations are 22% and 78%, respectively.

To reaffirm the boron content measured by SNMS, the Rutherford backscattering spectrometry (RBS) measurement and simulation were carried out by EAG Laboratories as shown in Fig. 4. The RBS is an accurate measurement method to determine the material content, independent of strain and defects. The RBS measurement was conducted with a grazing angle detector of 160°, where the sample's face was perpendicularly set to the incident He^{++} ion beam with an energy of 2.275 MeV. The peak intensity of boron could be observed even with the small nucleus of the B. Both boron and aluminum contents can be obtained by simulation fitting using the HYPRA program. The boron content of BAlN was determined to be 22% in excellent agreement with the SNMS result. Based on the XRD, SIMS, SNMS, and RBS measurements, the boron composition of the BAlN film is over 20% and homogeneous throughout the thickness of the film.

The sample was further characterized by transmission electron microscopy (TEM). The TEM sample was prepared using an FEI

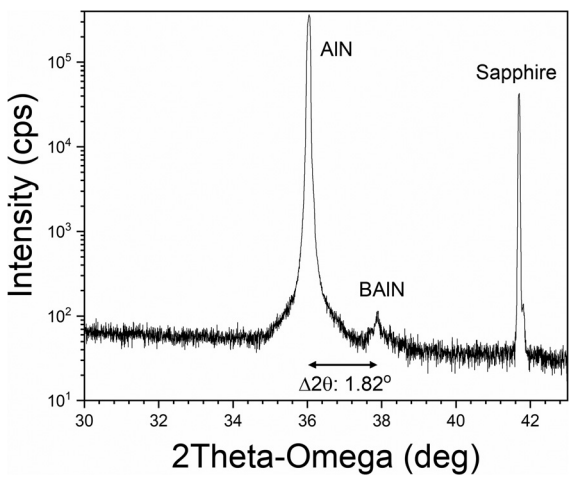

FIG. 2. The (002) 2θ–ω XRD scan showing the peaks of the AlN template, BAlN film, and sapphire substrate.

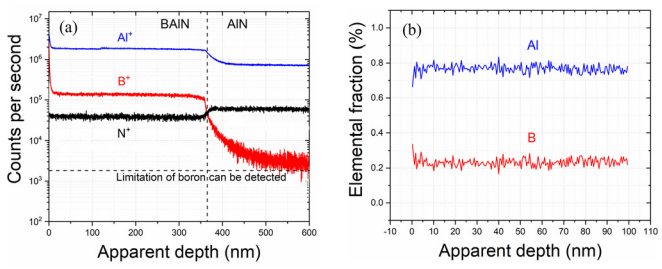

FIG. 3. (a) The SIMS depth profile of the BAlN film grown on the AlN/sapphire template. (b) The boron and aluminum contents measured by SNMS measurements.

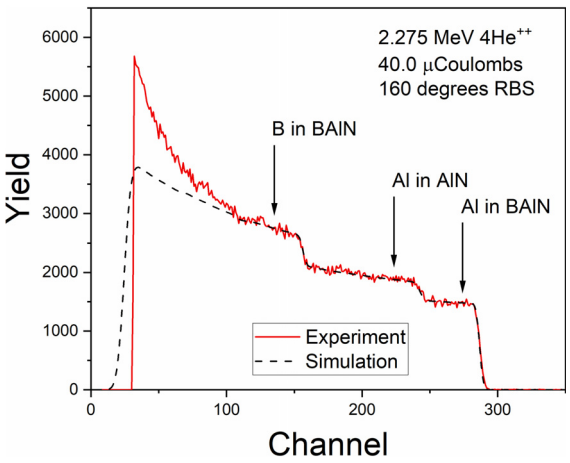

FIG. 4. Experimental and simulation RBS spectra of the sample.

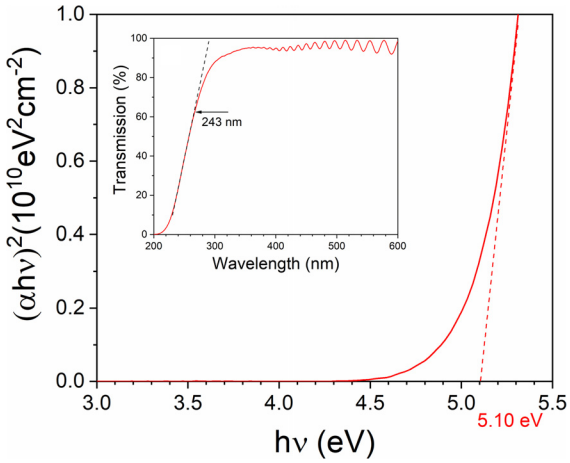

FIG. 6. The Tauc plot of the sample measured at RT and the inset shows the UV-Vis transmission spectrum.

Helios focused ion beam (FIB) system. The cross-sectional TEM was performed along the [1–100] zone axis with an operating voltage of 300 keV using a Themis Z system from Thermo Fisher Scientific. Figure 5(a) shows the sharp interface between the AlN template and the BAlN film, as well as a 5 nm thick wurtzite BAlN layer without crystal twinning according to the fast Fourier transform (FFT) image in Fig. 5(b). Above the 5 nm layer, the BAlN layer starts to show consideration defects with crystal twinning previously observed by Wang *et al.* in the wurtzite BAlN films with smaller boron contents.[10] Figures 5(c) and 5(d) show the FFT patterns of two different areas above the 5 nm wurtzite BAlN layer with additional diffraction spots from a mirror reflection of lattice planes. They show similar twin formation, suggesting the wurtzite structure with overlapping twin crystal structures tilted by 60 degree, one clockwise and the other anti-clockwise. The formation mechanism of the twin formation in the wurtzite BAlN layer could be due to stress and preferred growth orientations, which warrant further studies.

The inset of Fig. 6 shows the UV-Vis optical transmission spectrum of the sample. The transmission is high from visible to 280 nm. Below 280 nm, the transmission quickly reduces though

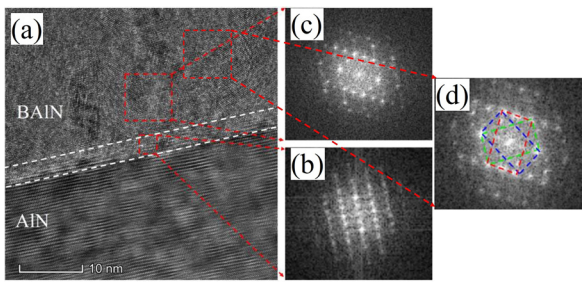

FIG. 5. (a) The cross-sectional TEM image in the vicinity of the BAlN/AlN interface where the white dashed lines indicate the 5 nm thick wurtzite BAlN layer without crystal twinning. The FFT images of (b) the 5 nm wurtzite BAlN layer without crystal twinning and (c) one area and (d) another area of the wurtzite BAlN region with crystal twinning.

showing tapering probably due to the high carbon impurity level in the BAlN film related to the use of TEB precursors amid MOCVD.[15] The corresponding Tauc plot is plotted in Fig. 6. The optical bandgap of the BAlN film was deduced to be 5.1 eV, which is in good agreement with the bandgap of $B_{0.22}Al_{0.78}N$ linearly interpolated based on the results calculated by the density functional theory using the Heyd, Scuseria, and Ernzerhof (HSE) hybrid functional.[18] The result indicates that the BAlN film in this study possesses a smaller bandgap as opposed to AlN despite a smaller lattice constant as predicted by the theoretical studies,[6,18] which contrasts drastically from the conventional InGaAlN material system.

In conclusion, we demonstrated a 360 nm single-phase wurtzite BAlN film with a record-high boron composition over 20% on an AlN/sapphire template by MOCVD. The growth was conducted at a temperature of 1010 °C and a pressure of 150 Torr with continuous flows of group-III precursors and ammonia, resulting in a growth rate of 2.2 μm/h. The RMS surface roughness of the BAlN film was 2.7 nm from the 5×5 μm^2 AFM image. The 2θ XRD scan shows that the film was free of phase separation and the 2θ angular separation between the BAlN and AlN peaks was 1.82°, based on which the boron composition was 30.9%. The SNMS and RBS experiments were carried out to investigate the boron composition, leading to a lower value of 22%. The TEM studies show that the BAlN film comprised a 5 nm thick layer free of crystal twinning at the BAlN/AlN interface; and the rest of the BAlN film had crystal twinning with lattice rotations of 60° clockwise and anti-clockwise. The optical transmission experiment exhibited that the bandgap of the BAlN film was 5.1 eV, which was smaller than that of AlN and consistent with theoretical predictions. The demonstration of the over 20% boron composition BAlN thin film with a large thickness can greatly facilitate the basic and applied research of the BAlN alloys for enhanced III-nitride devices.

The authors would like to thank the support of KAUST Baseline Funds No. BAS/1/1664-01-01, Competitive Research

Grant Nos. URF/1/3437-01-01 and URF/1/3771-01-01, and GCC Research Council No. REP/1/3189-01-01.

DATA AVAILABILITY

The data that support the findings of this study are available within the article.

REFERENCES

[1]X. Li, S. Wang, H. Liu, F. A. Ponce, T. Detchprohm, and R. D. Dupuis, Phys. Status Solidi B **254**, 1600699 (2017).
[2]T. T. Luong, Y. T. Ho, B. T. Tran, Y. Y. Woong, and E. Y. Chang, Chem. Vap. Deposition **21**, 33–40 (2015).
[3]B. T. Tran and H. Hirayama, Sci. Rep. **7**, 12176 (2017).
[4]M. Abid, T. Moudakir, G. Orsal, S. Gautier, A. E. Naciri, Z. Djebbour, J.-H. Ryou, G. Patriarche, L. Largeau, H. J. Kim, Z. Lochner, K. Pantzas, D. Alamarguy, F. Jomard, R. D. Dupuis, J.-P. Salvestrini, P. L. Voss, and A. Ougazzaden, Appl. Phys. Lett. **100**, 051101 (2012).
[5]A. Y. Polyakov, M. Shin, W. Qian, M. Skowronski, D. W. Greve, and R. G. Wilson, J. Appl. Phys. **81**, 1715–1719 (1997).
[6]M. Zhang and X. Li, Phys. Status Solidi B **254**, 1600749 (2017).
[7]X. Li, H. Xie, F. A. Ponce, J.-H. Ryou, T. Detchprohm, and R. D. Dupuis, Appl. Phys. Lett. **107**, 241109 (2015).
[8]H. Sun, F. Wu, Y. J. Park, T. M. Al tahtamouni, C.-H. Liao, W. Guo, N. Alfaraj, K.-H. Li, D. H. Anjum, T. Detchprohm, R. D. Dupuis, and X. Li, Appl. Phys. Express **11**, 011001 (2018).
[9]H. Sun, Y. J. Park, K.-H. Li, X. Liu, T. Detchprohm, X. Zhang, R. D. Dupuis, and X. Li, Appl. Surf. Sci. **458**, 949–953 (2018).
[10]S. Wang, X. Li, A. M. Fischer, T. Detchprohm, R. D. Dupuis, and F. A. Ponce, J. Cryst. Growth **475**, 334–340 (2017).
[11]M. Imura, Y. Ota, R. Banal, M. Liao, Y. Nakayama, M. Takeguchi, and Y. Koide, Phys. Status Solidi A **215**, 1800282 (2018).
[12]L. K. Teles, J. Furthmüller, L. M. R. Scolfaro, A. Tabata, J. R. Leite, F. Bechstedt, T. Frey, D. J. As, and K. Lischka, Physica E **13**, 1086–1089 (2002).
[13]L. Liljeholm and J. Olsson, Vacuum **86**, 466–470 (2011).
[14]T. Akasaka, Y. Kobayashi, and T. Makimoto, Appl. Phys. Lett. **91**, 041914 (2007).
[15]X. Li, S. Sundaram, Y. E. Gmili, F. Genty, S. Bouchoule, G. Patriache, P. Disseix, F. Réveret, J. Leymarie, J. P. Salvestrini, R. D. Dupuis, P. L. Voss, and A. Ougazzaden, J. Cryst. Growth **414**, 119–122 (2015).
[16]V. L. Solozhenko, D. Häusermann, M. Mezouar, and M. Kunz, Appl. Phys. Lett. **72**, 1691–1693 (1998).
[17]See https://www.hidenanalytical.com/wp-content/uploads/2016/07/Combined-SIMS-SNMS-Poster.pdf for the information about the secondary ion mass spectroscopy (SIMS) and the secondary neutral mass spectroscopy (SNMS) modes (accessed June 24, 2020).
[18]C.-H. Liao, F. Alqatari, and X. Li, preprint arXiv:2005.08274 (2020).
[19]A. Béré and A. Serra, Phys. Rev. B **65**, 205323 (2002).